TEKA Kom. Mot. Energ. Roln. – OL PAN, 2009, 9, 418–430

MODELLING THE PRESSURE DISTRIBUTION IN OIL FILM IN THE VARIABLE HEIGHT GAP BETWEEN THE VALVE PLATE AND CYLINDER BLOCK IN THE AXIAL PISTON PUMP

Tadeusz Złoto

Armii Krajowej Av.21, 42-200 Czestochowa, Poland, e-mail: zlotot@o2.pl
Institute of Machine Technology and Production of Automation
Czestochowa University of Technology

Summary. The pressure distribution of oil film at the smallest height of the gap occurring between the valve plate and cylinder block is given as a function of geometrical and working parameters of the axial piston pump. An analysis was performed using the finite element method implemented in a computer program developed by the author of the present paper.

Key words: pressure distribution, variable height gap, axial piston pump, computer program.

INTRODUCTION

Among many cooperating or adjacent surfaces of components in hydraulic machines there exist oil filled gaps. Phenomena occurring in these gaps are considered among the most important ones for the system behaviour. It follows not only from a substantial impact exerted by these phenomena on the energy balance in the hydraulic system, but also from their variety and mutual dependencies [Osiecki 1998].

One of the kinematical pairs affecting the efficiency of an axial piston pump is the valve plate – cylinder block system. When the pump is operating a gap filled with oil of small height appears between the rotating cylinder block with the set of cylinders and the valve plate. The gap can be either parallel [Stryczek 1995], which is the most desirable case, or of variable height [Jang 1997], which is a result of the imbalance between the hydrostatic forces pressing the cylinder block and valve plate towards each other and forces pressing them apart from each other. The present paper deals with the latter case, i.e. the gap of variable height. We shall examine how the pressure distribution in the oil film in the gap where its height is the smallest varies according to the leveling of the cylinder block and exploitation parameters of the pump.

ANALYSIS OF HEIGHT OF WEDGE GAP BETWEEN THE VALVE PLATE AND CYLINDER BLOCK

The general case of cylinder block placement with respect to the valve plate in the pump is depicted in Fig. 1. Individual cylinder block settings with respect to the valve plate, depicted in Fig. 2, can be considered theoretically.

For a further analysis it is necessary to determine the theoretical distribution of heights of wedge gap between the valve plate and cylinder block [Zloto 1997]. The lower surface of the valve plate and the upper surface of cylinder block are flat. In the case, when there are no displacements, these surfaces adhere and their axes are the same (Fig. 2d). The valve plate does not move. The cylinder block rotates along its axis.

In the initial position for the general case the cylinder block and valve plate surfaces are placed with respect to each other like in the case depicted in Figure 1. The coordinate systems x and x_1 are assigned to appropriate surfaces. The directional versor (its components) of the cylinder block surface in the x_1 coordinate system may be written as:

$$\underset{1}{\bar{n}} = \left[0, \quad 0, \quad 1\right]^T. \tag{1}$$

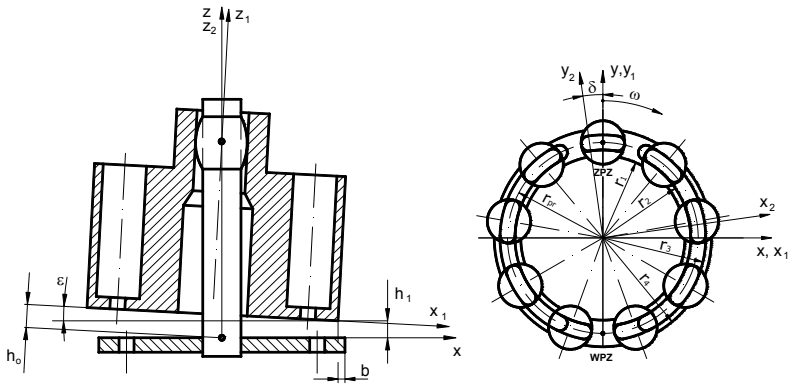

Fig. 1. A general case of cylinder block placement with respect to the valve plate

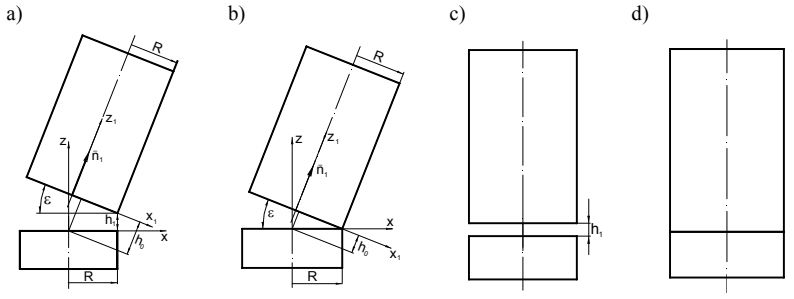

Fig. 2. Specific cases of cylinder block placement with respect to the valve plate: a) b = 0; b) b = 0, $h_1 = 0$; c) ε = 0, b = 0; d) ε = 0, b = 0, $h_1 = 0$

In order to write the equation for this plane in the x coordinate system related to valve plate it is necessary to write this versor in that coordinate system. The distance of cylinder block plane from the origin of x coordinate system is equal to:

$$h_0 = (R \pm b)\sin\varepsilon + h_1 \cos\varepsilon. \tag{2}$$

An additional coordinate system x_2 was introduced, which at the initial time instant $\delta = 0$ is equivalent to the x coordinate system and is related to cylinder block. This coordinate system rotates with respect to the x system along with the common rotation axis $z = z_2$ at the angle δ.

In order to write down the versor components of cylinder block rotation (directional cosines) in the valve plate system it is not necessary to take into account the mutual displacement of the origins of the introduced coordinate systems.

Therefore it is possible to make a transformation from the x_1 coordinate system to the x_2 coordinate system (Fig. 3a) using the rotation matrix (in order to give a formulation for this matrix the origins of the coordinate systems were placed at a single point):

$$\left[\underset{2-1}{M}\right] = [2, \quad -\varepsilon] = \begin{bmatrix} \cos\varepsilon & 0 & \sin\varepsilon \\ 0 & 1 & 0 \\ -\sin\varepsilon & 0 & \cos\varepsilon \end{bmatrix}, \tag{3}$$

and for transformation into the x coordinate system (Fig. 3b):

$$\left[\underset{0-2}{M}\right] = [3, \quad -\delta] = \begin{bmatrix} \cos\delta & -\sin\delta & 0 \\ \sin\delta & \cos\delta & 0 \\ 0 & 0 & 1 \end{bmatrix}. \tag{4}$$

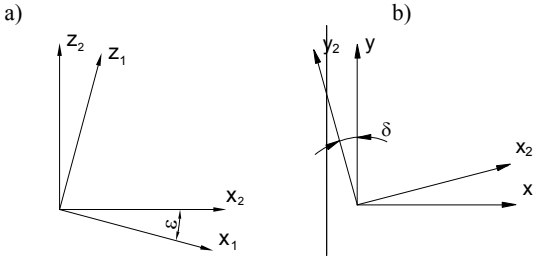

Fig. 3. Transformations between the coordinates systems a) related to cylinder block, b) related to valve plate

The directional versor of the cylinder block plane in the x coordinated system related to valve plate can be written as:

$$\bar{n} = [3, \quad -\delta][2, \quad -\varepsilon]\bar{n}_1 = [\cos\delta \sin\varepsilon, \quad \sin\delta \sin\varepsilon, \quad \cos\varepsilon]^T. \tag{5}$$

Therefore the equation for cylinder block plane in the x coordinate system may be written as:

$$x\cos\delta \sin\varepsilon + y\sin\delta \sin\varepsilon + h\cos\varepsilon - h_0 = 0. \tag{6}$$

The height of gap between the planes valve plate – cylinder block measured in the direction of z axis may be determined from the equation:

$$h = -x\cos\delta \cdot tg\varepsilon - y\sin\delta \cdot tg\varepsilon + (R+b)tg\varepsilon + h_1. \tag{7}$$

Because the valve plate plane is limited with a circle, so it is useful to give the coordinates of points belonging to this plane in the form:

$$x = r\sin\varphi,\ y = r\cos\varphi. \tag{8}$$

The gap height may vary from the minimal to maximal value and is considered in dependence on spherical coordinates r and φ, cylinder block bias angle ε, tangency angle δ for minimal gap height h_1 and cylinder block radius R. The quantity b as radius beat does not occur in practice.

From literature and experimental studies [Zloto 2007] it follows, that the tangency point between the cylinder block and valve plate occurs below the coordinate x, what confirms the occurence of the load forces in this quarter of trajectories.

APPROXIMATE SOLUTION OF THE REYNOLDS EQUATION USING THE FINITE ELEMENT METHOD

The operation of the valve plate-cylinder block system resembles the operation of a hydrostatic axial bearing [Ivantysyn and Ivantysynova 2001].

According to the hydrodynamic lubrication theory, distribution of pressure in the frontal gap of a hydrostatic bearing can be described by the Reynolds equation [Pasynkov and Posvianski 1993]:

$$\frac{\partial}{\partial x}\left(\frac{h^3\rho}{\mu}\frac{\partial p}{\partial x}\right) + \frac{\partial}{\partial y}\left(\frac{h^3\rho}{\mu}\frac{\partial p}{\partial y}\right) = 6\frac{\partial}{\partial x}(\rho uh) + 6\frac{\partial}{\partial y}(\rho vh) + 12\rho w, \tag{9}$$

where: p is the pressure in the bearing gap, h is the gap height, ρ is the lubricating oil density, μ is the dynamic lubricant viscosity, and u, v, w denote the components of peripheral velocity by the given angular velocity ω and the radius vector r of the cylinder block with respect to the axes x,y,z in the Cartesian coordinate system.

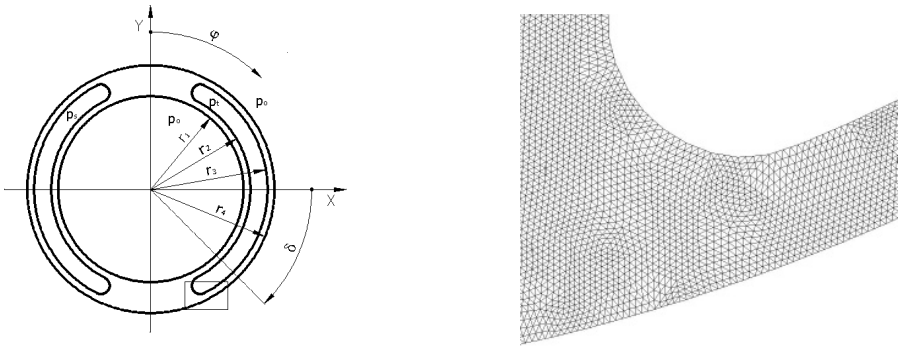

Fig. 4. Main dimensions of the computational domain of the valve plate and part of the finite element mesh

The Reynolds equation (9) holds under the following assumptions:

- the flow in the frontal gap is laminar,
- fluid friction takes place between the cooperating surfaces,
- the lubricant is an incompressible Newtonian fluid,

- the pressure is constant in the direction orthogonal to the surface,
- the cooperating surfaces are rigid.

Analytical solution of equation (9) is quite complicated, particularly for surfaces of more complex shape. Therefore, the equation was solved numerically using the finite element method. In this method geometric domain Ω under consideration is divided into finite elements, that is disjoint geometric figures of simple shape, such as triangles or quadrilaterals (Fig. 4).

These simple figures constitute a mesh where their vertices are the mesh nodes. Approximate solution of equation (9) is represented as a linear combination of some functions N_j and values of the pressure p_j in mesh nodes:

$$p(x,y)=\sum_{j=1}^{L} N_j(x,y)p_j, \tag{10}$$

where: L denotes the number of nodes in the mesh. The nodal values p_j are the unknowns of the problem and after they have been determined it is possible to calculate the pressure in any point of the domain.

The functions N_j, called basis or shape functions, are used for interpolation of the pressure within a finite element. The shape function N_j, associated with the node of the index j, has the property:

$$N_j\left(x_k,y_k\right)=\begin{Bmatrix}1, & j=k\\ 0, & j\neq k\end{Bmatrix}, \tag{11}$$

i.e. it equals one in this node, whereas it is equal to zero in the other nodes. Given that an element under consideration has vertices in nodes i, j, m, the shape function associated with the node i equals [12]:

$$N_i(x,y)=\frac{a_i+b_ix+c_iy}{2A}, \tag{12}$$

where: $a_i=x_jy_m-x_my_j$, $b_i=y_j-y_m$, $c_i=x_m-x_j$, and A denotes the element surface area. The other shape functions can also be calculated from formula (12) after cyclic permutation of the indices, e.g. to j, m, i.

Approximate solution obtained numerically usually fails to satisfy the partial differential equation (9). The magnitude of this discrepancy can be measured by the residual, which is the result of the substitution of the approximate solution for the exact one. For the Reynolds equation the residual is given as:

$$r=6\frac{\partial}{\partial x}(\rho uh)+6\frac{\partial}{\partial y}(\rho vh)+12\,\rho w-\frac{\partial}{\partial x}\left(\frac{h^3\rho}{\mu}\frac{\partial p}{\partial x}\right)-\frac{\partial}{\partial y}\left(\frac{h^3\rho}{\mu}\frac{\partial p}{\partial y}\right)\neq 0. \tag{13}$$

The Galerkin weighted residual [Zienkiewicz and Morgan1983] method was applied in this work to derive finite element equations. It is required that:

$$\int_{\Omega} rN_i\,dxdy=0 \quad \text{for } i=1,2,...,L, \tag{14}$$

i.e. that the residual be orthogonal to each shape functions defined in the mesh.

Substituting the residual (13) in the equation (14), integration by parts and some reordering results in the following system of equations:

$$\int_{\Omega}\frac{h^3\rho}{\mu}\left(\frac{\partial p}{\partial x}\frac{\partial N_i}{\partial x}+\frac{\partial p}{\partial y}\frac{\partial N_i}{\partial y}\right)dxdy=\int_{\Omega}N_i\left(6\frac{\partial}{\partial x}(\rho uh)+6\frac{\partial}{\partial y}(\rho vh)+12\,\rho w\right)dxdy,\quad i=1,2,...,L. \tag{15}$$

Derivatives of the approximate solution with respect to spatial coordinates appear in equation (15). They can be represented using derivatives of the shape functions and the nodal pressure values as:

$$\frac{\partial p}{\partial x} = \sum_{j=1}^{N} \frac{\partial N_j}{\partial x} p_j, \quad \frac{\partial p}{\partial y} = \sum_{j=1}^{N} \frac{\partial N_j}{\partial y} p_j. \tag{16}$$

For triangular elements used in this paper derivatives of the shape functions are respectively equal to:

$$\frac{\partial N_i}{\partial x} = \frac{b_i}{2A}, \quad \frac{\partial N_i}{\partial y} = \frac{c_i}{2A}. \tag{17}$$

Substituting the derivatives from (16) into (17) gives the following system of algebraic equations:

$$\sum_{j=1}^{L} p_j \int_{\Omega} \frac{h^3 \rho}{\mu} \left(\frac{\partial N_j}{\partial x} \frac{\partial N_i}{\partial x} + \frac{\partial N_j}{\partial y} \frac{\partial N_i}{\partial y} \right) dxdy = \int_{\Omega} N_i \left(6 \frac{\partial}{\partial x} (\rho uh) + 6 \frac{\partial}{\partial y} (\rho vh) + 12 \rho w \right) dxdy, \quad i = 1,2,...,L. \tag{18}$$

This is a system of L equations with L unknowns p_j, which can be represented in a more compact manner in matrix-vector notation as:

$$\mathrm{Ap} = \mathrm{b}, \tag{19}$$

where:

$$a_{ij} = \int_{\Omega} \frac{h^3 \rho}{\mu} \left(\frac{\partial N_j}{\partial x} \frac{\partial N_i}{\partial x} + \frac{\partial N_j}{\partial y} \frac{\partial N_i}{\partial y} \right) dxdy, \quad i, j = 1,2,...,L, \tag{20}$$

$$b_i = \int_{\Omega} N_i \left(6 \frac{\partial}{\partial x} (\rho uh) + 6 \frac{\partial}{\partial y} (\rho vh) + 12 \rho w \right) dxdy, \quad i = 1,2,...,L. \tag{21}$$

This system is global. Analogous local systems of equations can be written for all finite elements, with the only difference lying in summing in the range $i = 1,2,3$ and in integration over the element area of only those shape functions that are associated with its nodes.

COMPUTER IMPLEMENTATION OF THE FINITE ELEMENT METHOD AND SIMULATION RESULTS

The finite element method for the Reynolds equation was implemented in a computer program. It was written in the C++ programming language based upon an existing software library of reusable components facilitating programming of the finite element method [Nagorka and Sczygiol 2004].

Finite element computations usually consist of:

- reading the mesh and problem data from files,
- building the system of equations (19) as the result of assembling contributions from individual elements,
- imposition of boundary conditions,
- solution of the resulting equation system,
- saving the results to files, visualization, etc.

Coefficients of the matrix and the right-hand side vector in equation system (19) involve integrals of shape functions or their derivatives, oil data, gap height and velocity components. The derivatives in (20) can be calculated from formula (17) and are constant within an element. However, variation of the height is non-polynomial and analytical evaluation of the integral (20) is troublesome. Similarly, derivatives of velocity and height in (21) make the integral difficult to evaluate. Therefore, numerical integration was used to calculate matrix and vector elements in system (19). Gaussian quadrature formulas were applied with points and weights taken from [Cools 2003].

The coefficient matrix in the system of equations (19) is sparse. Each matrix row corresponds to a single mesh node, and the number of non-zero coefficients in the row depends on the number of neighbor nodes connected with the given node by element edges, which is small. Keeping all the square matrix in memory would be waste of resources. In the computer program special data structures were applied to store only non-zero terms, thereby greatly reducing the memory consumption.

Solution of the system of algebraic equation (19) is by far the most time-consuming part of computations. Generally, the equations are nonlinear. However, in this work oil properties were assumed to be independent of pressure, hence system (19) is linear. To solve such a system one of the iterative solution methods, namely the conjugate gradient method with the Jacobi preconditioner [Barret *et al.* 1994] was applied. The advantages of this method are much better efficiency when compared to classical direct methods, such as Gaussian elimination on dense or sparse matrices, and feasibility of efficient use of sparse matrix data structures.

The developed computer program accepts input data and saves the results in file formats compliant with a software package NuscaS [Sczygiol *et al*. 2002], used for mesh generation, preprocessing, visualization, etc.

The accuracy of the finite element solution depends on mesh density: the smaller the elements, the better accuracy. This is particularly important in place where rapid variation of pressure occurs, close to the site of the smallest bearing gap height.

An example of the adapted mesh covering the domain of a bearing is presented in Figs 5-7. The mesh is the result of adaptive refinement done during solution of a problem with the pressure peak at $\varphi = 135^{\circ}$. Subsequent figures show greater and greater zoom on the mesh region near the peak. Density grading towards the external boundary of the bearing was achieved automatically after six iterations of adaptive refinement.

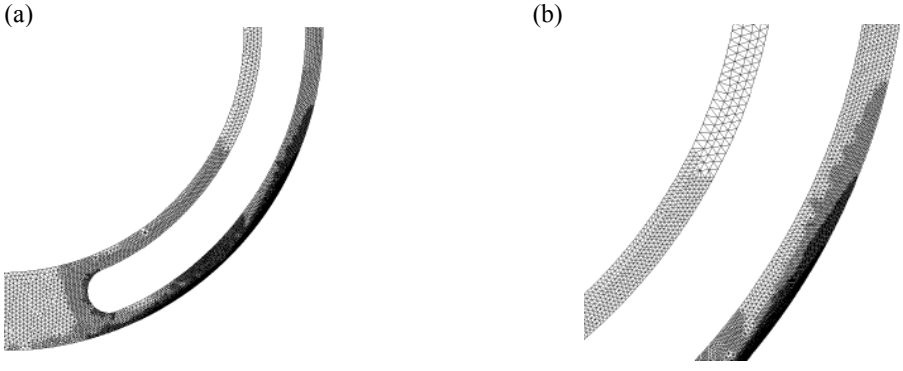

Fig. 5. Local increase in grid density in the area of the „peak" pressure:
(a) outlook of the pressure port, (b) zoom of graded mesh

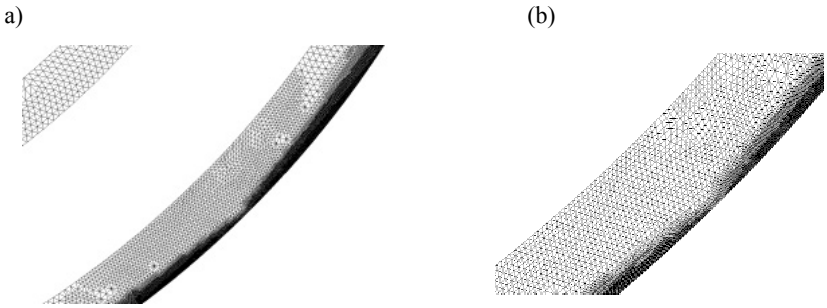

Fig. 6. Local increase in grid density in the area of substantial variations of pressure values: successive zooms (a) and (b)

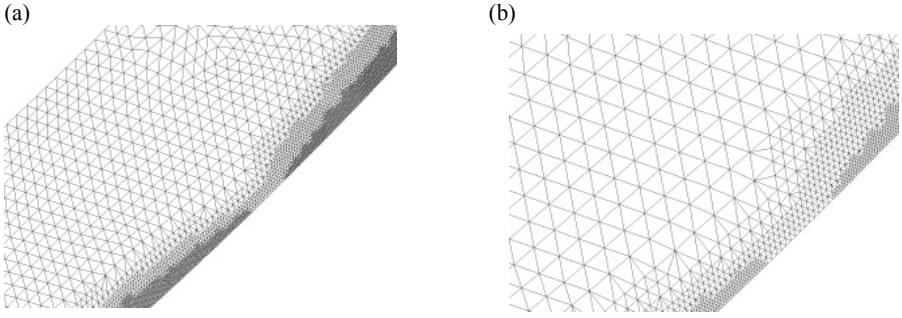

Fig. 7. Local increase in grid density in specific areas of pressure variations: successive zooms (a) and (b)

Simulations were performed on meshes from a sequence with increasing element density until convergence was reached, i.e. until the result on the two consecutive meshes were similar enough. Final computations were done on the densest mesh including 80194 nodes and 154336 triangular elements with linear interpolation of the pressure.

Distribution of pressure in the oil film inside the variable-height gap on the valve plate was analyzed using the finite element method, the developed computer program and geometric and exploitation data of the valve plate-cylinder block system in an axial piston pump under the assumption of calculational model with rotating plate imitating the operating cylinder block.

The following input parameters were assumed in the developed computational model (Fig. 4):

- in the pressure port the pressure $p_t = 32$ MPa,
- in the suction port the pressure $p_s = 0$ MPa,
- outside and inside the valve plate the pressure $p_o = 0$ MPa,
- angular velocity of the cylinder block $\omega = 157$ rad/s
- dynamic viscosity of the oil $\mu = 0.0252$ Pas,
- the angle of the smallest height of the gap with respect to the axis x $\delta = 0.785$ rad,
- the angle of the cylinder block with respect of the valve plate $\varepsilon = 0.000523$ rad,
- minimal gap height $h_{min} = 3*10^{-7}$ m,
- characteristic radii of the valve plate are $r_1 = 0.0284$ m, $r_2 = 0.0304$ m, $r_3 = 0.0356$ m, and $r_4 = 0.0376$ m.

In the model boundary conditions it was assumed, that cavitation prcesses begin with underpressure approximately equal to – 0.05 MPa [Osiecki 1998].

In Fig. 8 the calculated distribution of oil film pressure on the valve plate is presented. Pressure variation in the vicinity of the lowest bearing gap height is of greatest interest. In the confusor part of the gap (where the height decreases) an overpressure peak is visible, whereas in the diffusor part a specific value of underpressure limited with cavitation phenomenon occurs. Peripheral section at the radius 0.03715 m with the greatest pressure peaks is depicted in Fig. 9.

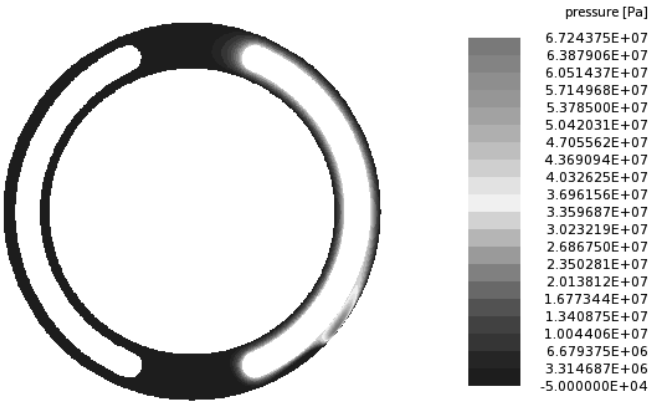

Fig. 8. Oil film pressure distribution on the valve plate

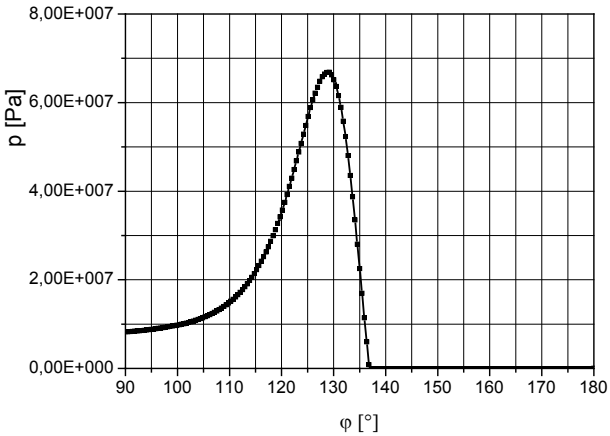

Fig. 9. Pressure waveforms of the oil film in the vicinity of the smallest height gap of the circumferential section at the radius r = 0.03715 m depending on the cylinder block revolution

The calculation results were confirmed using commercial software FLUENT. The confirmation of occurrence of overpressure "peak" in the kinematical pair hydrostatic slipper- swash plate in the neighbourhood of the minimum gap height is depicted in Figure 10 [Lasaar and Ivantysynova 2002].

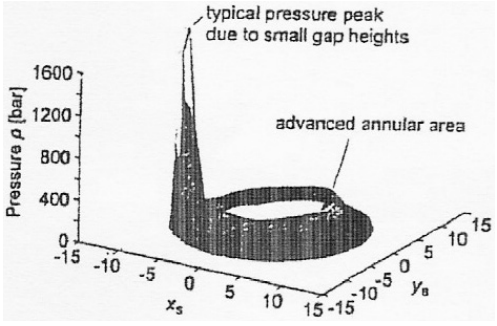

Fig. 10. Pressure field under slipper [Lasaar and Ivantysynova 2002]

In literature [Kunze and Brunner 1996] attention is paid to the occurence of cavitation phenomenon in axial piston pumps. In Figure 11 the damages of the outer parts of cylinder block cylinder outlets due to cavitation phenomenon.

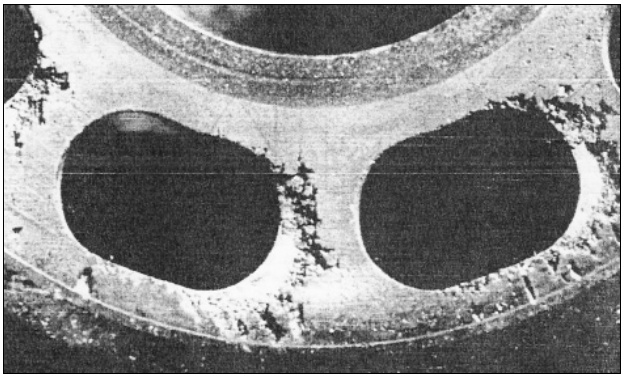

Fig. 11. Damages of the outer parts of cylinder block cylinder outlets [Kunze and Brunner 1996]

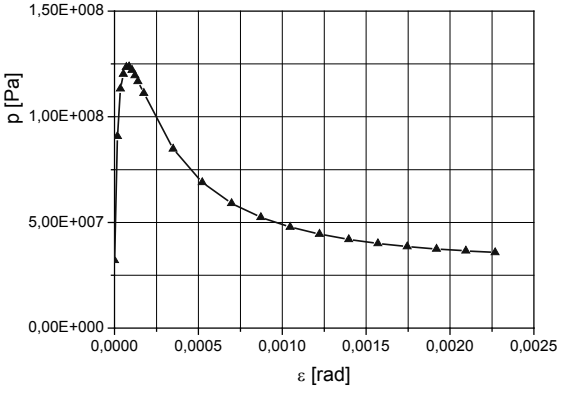

Fig. 12. Values of maximum pressure of oil film depending on the cylinder block inclination angle ε

It is supposed, that the cause of the cavitation phenomenon is the occurence of underpressure in the diffusor gap in the neighbourhood of the minimum gap height.

In the analysis of the pressure distribution the influence of the geometrical and exploitation parameters of the cylinder block-valve plate system on the pressure increase in the smallest gap height area was taken into consideration.

In Fig. 12 the effect of the cylinder block inclination with respect to the valve plate is shown. As the inclination angle increases, the peak values of the maximum pressure decrease. The greatest values occur for small angles ε.

In Fig. 13 the influence of exploitation parameters on the maximum pressure values is depicted.

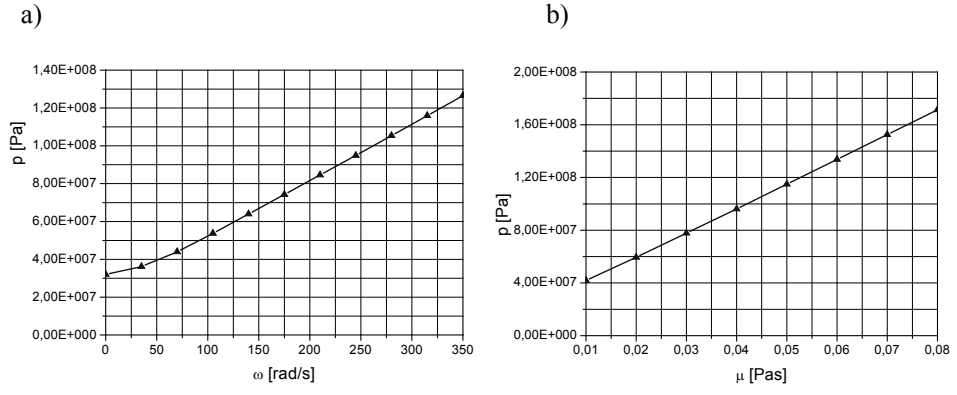

Fig. 13. Values of maximum pressure of oil film depending: a) on the cylinder block angular velocity ω, b) on the dynamic viscosity coefficient μ of oil

An increase in the angular velocity and in the dynamic viscosity coefficient causes a linear increase in the values of the maximum pressure of the oil film. As the minimum gap h_1 increases, the values of overpressure "peaks" decrease, what is depicted in Figure 14.

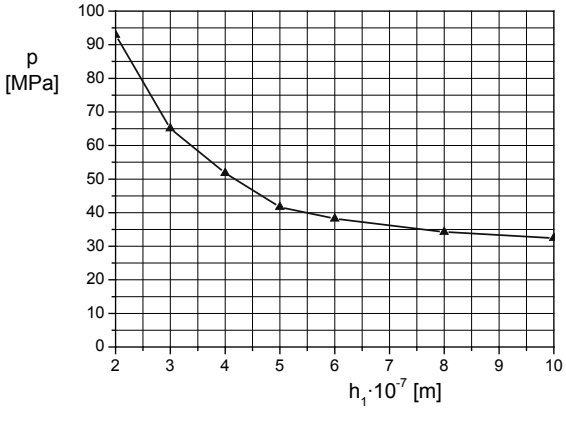

Fig. 14. The dependence of maximum pressure p_{max} on minimum gap height h_1

CONCLUSIONS

The present investigations lead to the following conclusions:

1. The finite element method combined with numerical methods enables the solution of the Reynolds equation in order to determine the oil film pressure in variable height gaps between co-operating elements.

2. The distribution of the maximum pressures of the oil film in the area of the smallest height gap are dependent on the selected geometrical and exploitation parameters of the pump. As the inclination angle of the cylinder block decreases and the angular velocity and the dynamic oil viscosity coefficient increase, the values of the maximum pressure increase. On the other hand, the values of underpressure are limited with cavitation phenomenon, which occurs already at underpressure – 0.05 Mpa.

REFERENCES

Barrett R., Berry M., Chan T.F., Demmel J., Donato J., Dongarra J., Eijkhout V., Pozo R., Romine C., Vorst H.V., 1994: Templates for the Solution of Linear Systems, Building Blocks for Iterative Methods. 2nd Edition, SIAM, Philadelphia, PA. Cools R., 2003: An Encyclopaedia of Cubature Formulas J. Complexity, 19, 445-453.

Ivantysyn J., Ivantysynova M., 2001: Hydrostatic Pumps and Motors, Akademia Books International. New Delhi.

Jang D. S., 1997: Verlustanalise an Axialkolbeneinheiten. Dissertation RWTH Aachen.

Kunze T., Brunner H., 1996: Vibroakustische und optische Untersuchung der Kavitation bei Axialkolbenmaschinen. Ölhydraulik und Pneumatik, 40, Nr 8, 542-546.

Lasaar R., Ivantysynova M., 2002: Advanced Gap Design - Basis for Innovative Displacement Machines. 3-rd International Fluid Power Conference. Aachen, Vol. 2, 215-230.

Nagorka A., Sczygiol N., 2004: Implementation aspects of a recovery-based error estimator in finite element analysis, [in] Lecture Notes in Computer Science, 3019, Wyrzykowski R.et al. (Eds.), 722-729.

Osiecki A., 1998: Hydrostatyczny naped maszyn. WNT, Warszawa.

Pasynkow R.M., Posvianski W.S., 1993: Czisliennoje rieszienie urawnienia Riejnoldsa s uczietom pieriemiennoj wiaskosti żidkosti. Viestnik Maszinostrojenia Nr 9, 26-29.

Sczygiol N., Nagorka A., Szwarc G., 2002: NuscaS - autorski program komputerowy do modelowania zjawisk termomechanicznych krzepnięcia. Polska Metalurgia w latach 1998 – 2002. Wydawnictwo Naukowe AKAPIT, 243-249.

Stryczek S., 1995: Naped Hydrostatyczny, tom 1. WNT, Warszawa 1995.

Zienkiewicz O.C. and Morgan K., 1983: Finite elements and approximation. John Wiley & Sons, Inc.

Zienkiewicz O. C., Taylor R.L., 2000: The Finite Element Method. Butterworth-Heinemann. Oxford.

Zloto T., 2007: Modelowanie odciazenia hydrostatycznego i analiza zjawisk przeplywowych w szczelinie rozrzadu tarczowego pompy wielotloczkowej osiowej. Monografie nr 133. Wyd. Politechniki Czestochowskiej, Czestochowa.

MODELOWANIE ROZKŁADÓW CIŚNIENIA W FILMIE OLEJOWYM W SZCZELINIE KLINOWEJ ROZRZĄDU POMPY WIELOTŁOCZKOWEJ

Streszczenie. W pracy przedstawiono rozkłady ciśnienia filmu olejowego w otoczeniu najmniejszej wysokości szczeliny klinowej występującej w zespole rozrządu tarczowego w zależności od parametrów geometryczno - eksploatacyjnych pompy wielotłoczkowej osiowej. Do analizy wykorzystano metodę elementów skończonych opracowując własny program komputerowy.

Słowa kluczowe: rozkłady ciśnienia, szczelina klinowa, pompa wielotłoczkowa, program komputerowy.